Structural Engineering and Mechanics, *Vol. 67, No. 1 (2018) 93-104*
DOI: https://doi.org/10.12989/sem.2018.67.1.093

Seismic performance of RC short columns with light transverse reinforcement

Cao Thanh Ngoc Tran*[1] and Bing Li[2a]

[1]*Department of Civil Engineering, International University, Vietnam National University, Hochiminh, Vietnam*
[2]*School of Civil and Environment Engineering, Nanyang Technological University, 639798, Singapore*

(Received May 26, 2017, Revised March 28, 2018, Accepted March 29, 2018)

Abstract. The seismic behavior of reinforced concrete (RC) short columns with limited transverse reinforcement is investigated in this paper through an experimental program. The experimental program consists of four small-scale RC columns with an aspect ratio of 1.7, which are tested to the axial failure stage. The cracking patterns, hysteretic responses, strains in reinforcing bars, displacement decomposition and cumulative energy dissipation of the tested specimens are reported in detail in the paper. The effects of column axial load are investigated to determine how this variable might influence the performance of the short columns with limited transverse reinforcement. Brittle shear failure was observed in all tested specimens. Beneficial and detrimental effects on the shear strength and drift ratio at axial failure of the test specimens due to the column axial load are found in the experimental program, respectively.

Keywords: reinforced concrete; short column; light transverse reinforcement; column axial load; drift ratio at axial failure

1. Introduction

The catastrophic failure of reinforced concrete columns with light transverse reinforcement reported in recent post-earthquake investigations (EERI 2012, 2013, 2016 and 2017) has triggered the interest of the research community for such columns. Excessive shear deformation in non-seismically detailed RC columns has been extensively reported in these investigations. This may lead to shear and axial failures; and full collapse of structures. The pioneers in this area, namely Yoshimura and Yamanaka (2002), Yoshimura and Nakamura (2003), Yoshimura *et al.* (2003), Lynn (2001), Nakamura and Yoshimura (2002), Ousalem (2006), Sezen (2008), Ghannoum and Moehle (2012a), Ghannoum and Moehle (2012b), Sharma *et al.* (2012), Tran (2012), Koçak (2013), LeBorgne and Ghannoum (2014), Wibowo *et al.* (2014), Koçak (2015), and Tran and Li (2015) have provided a better understanding of the collapse mechanisms of RC columns with limited transverse reinforcement.

Tran and Li (2015) conducted an experimental program on RC columns with light transverse reinforcement subjected to seismic loading to study the backbone curves of such columns. In this experimental program, four non-seismically detailed RC short column with aspect ratio of 1.7 (lower than 2.0) had been tested to the point of axial failure. The column axial loads applied in these test specimens were 0.2 and $0.35f'_cA_g$. The test results indicated that the column axial load played an important role in the seismic behavior of reinforced concrete short columns with light transverse reinforcement. It was found having a detrimental effect on the drift ratio at axial failure and maximum energy dissipation capacity of test specimens. However, the shear strength and initial stiffness increased with an increase in column axial load. In this experiment program, only two levels of column axil load were investigated. Therefore, to further explore the effects of the column axial load to the seismic behavior of reinforced concrete short columns with light transverse reinforcement, further experimental studies on this area are needed.

An experimental study is conducted in this research. Four small-scale RC short columns with light transverse reinforcement are tested to investigate the seismic behavior of these columns. The tested specimens have similar details with Tran and Li's specimens (2015). Other two levels of column axial loads of 0.05 and $0.50f'_cA_g$ are investigated in this study to further explore the effects of column axial loads to the seismic behavior of such short columns.

2. Experimental studies

2.1 Specimen details

The schematic dimensions and detailing of test specimens are presented in Fig. 1 and Table 1. The test specimens have similar reinforcement details with Tran and Li (2015)'s ones. Both square and rectangular specimens have an aspect ratio of 1.7. The only difference between the test specimens and Tran and Li (2015)'s ones is the column axial load. Two levels of column axial load investigated in Tran and Li (2015)'s studies were 0.2 and $0.35f'_cA_g$. In this experimental study, additional two levels of column axial load of 0.05 and $0.5f'_cA_g$ are investigated to further explore

*Corresponding author, Lecturer
E-mail: tctngoc@hcmiu.edu.vn
[a]Associate Professor
E-mail: cbli@ntu.edu.sg

ISSN: 1225-4568 (Print), 1598-6217 (Online)

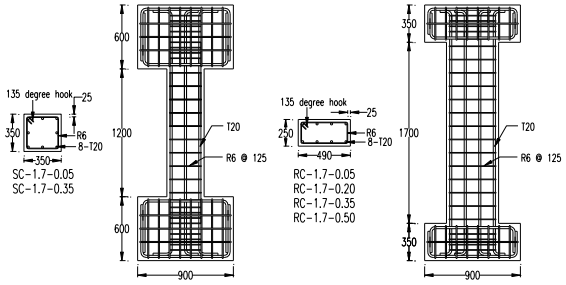

Fig. 1 Reinforcement details of test specimens (in mm)

Table 1 Summary of test specimens

Specimen	Longitudinal Bars	Transverse Bars	f_c' MPa	$b \times h$ mm×mm	L mm	$\frac{P}{f_c' A_g}$	V_u kN	V_n kN
SC-1.7-0.05	8-T20	2-R6@125	29.8	350 × 350	1200	0.05	303.2	209.8
SC-1.7-0.50			26.4			0.50	375.2	366.7
RC-1.7-0.05			32.5	250 × 490	1700	0.05	279.2	239.7
RC-1.7-0.50			26.8			0.50	337.5	394.9

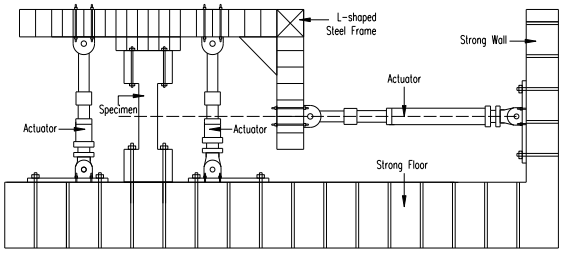

Fig. 2 Experimental Setup

the effects of column axial loads for both square and rectangular short columns. The longitudinal reinforcements of tested specimens consist of 8-T20 deformed bars. R6 bars at 125 mm spacing are provided for transverse reinforcement of all tested specimens. T20 and R6 bars have yield strength (f_y) of 408 MPa and 393 MPa, respectively. The theoretical flexural strengths V_u and nominal shear strengths V_n of the test specimens are tabulated in Table 1. The values of V_u and V_n of the test specimens were estimated in accordance with the recommendations provided by ACI 352 (2002) and ASCE/SEI 41's suggestion (2007), respectively.

2.2 Test setup and procedure

A double curvature bending condition is applied for these test specimens as shown in Fig. 2. A 100 ton capacity actuator mounted onto a reaction wall was used to apply reversible horizontal loads in a quasi-static fashion to the top of the column. The rotation was allowed by the pinned connections at both ends of the actuator. Four post-tensioned bolts were used to fix the base of test specimens to a strong floor. The procedure consisting of displacement-controlled steps is used for the applied lateral loading. This procedure is illustrated in Fig. 3. Two 100 ton capacity actuators were used to apply the column axial load to test specimens. A slowly displacement-controlled process is used to apply the axial load to the tested specimens. During the testing process, the vertical actuators are adjusted

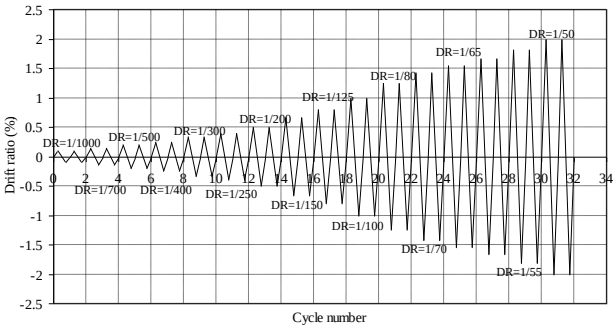

Fig. 3 Loading procedure

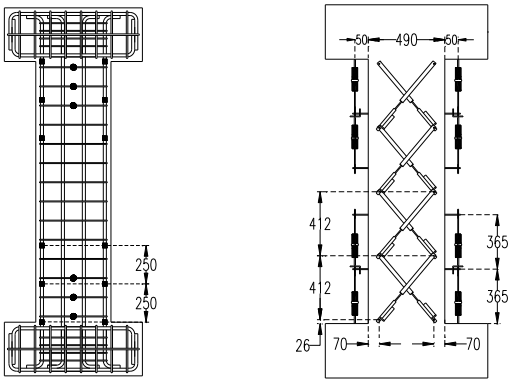

(a) (b)

Fig. 4 Typical strain gauge and LVDT locations (in mm)

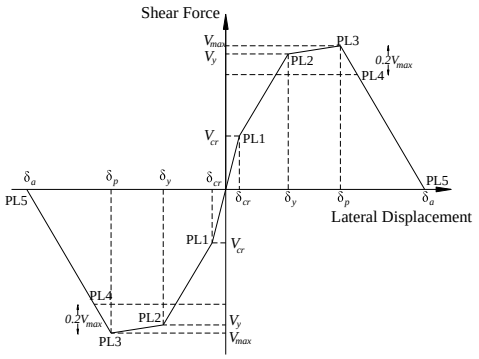

Fig. 5 Definition of performance levels

manually after each load step to maintain the designated level of column axial load. Throughout the tests, the strain in steel bars, shear and flexure deformations at the critical regions of the specimens were measured using the both internally and externally measuring devices as shown in Fig. 4.

3. Experimental results

This part of the paper presents the experimental results of the test specimens. Experimental results obtained include the measured hysteretic response (shear force versus lateral displacement), the observed cracking patterns, the strain readings from the reinforcing bars, the decomposition of horizontal displacements and the cumulative energy dissipations. The results of all test specimens will be

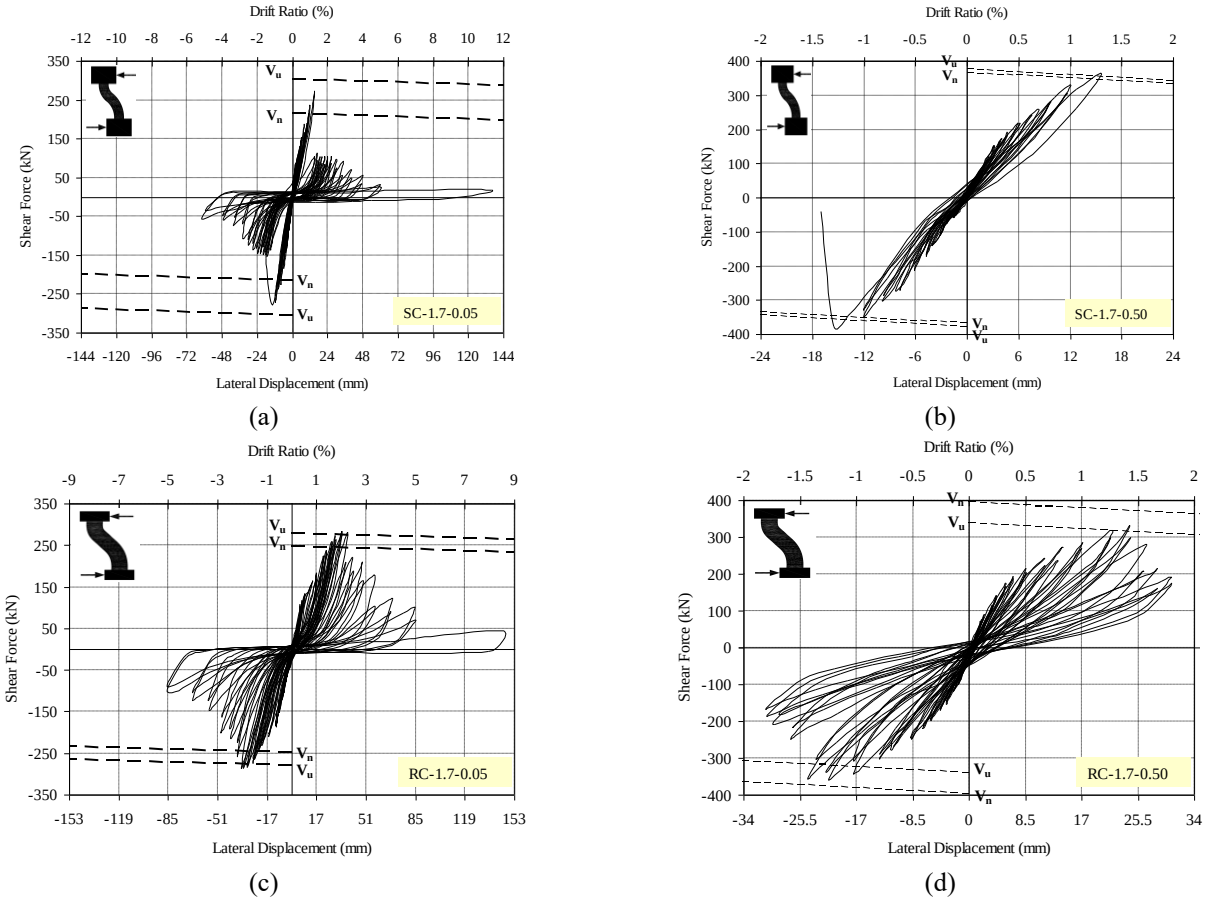

Fig. 6 Hysteretic responses of test specimens

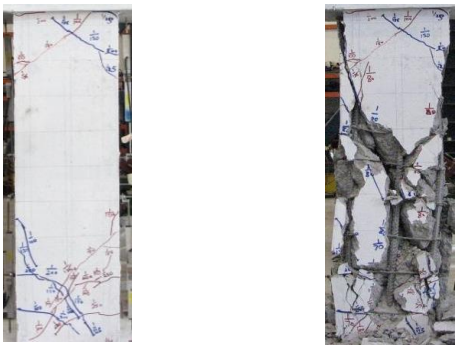

(a) at PL3 (b) at PL5

Fig. 7 Cracking patterns of SC-1.7-0.05

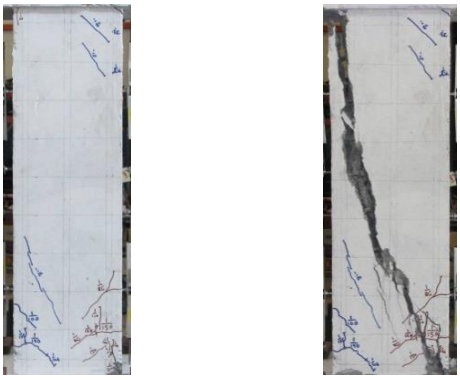

(a) at PL3 (b) at PL5

Fig. 8 Cracking patterns of SC-1.7-0.50

(a) at PL3 (b) at PL5

Fig. 9 Cracking patterns of RC-1.7-0.05

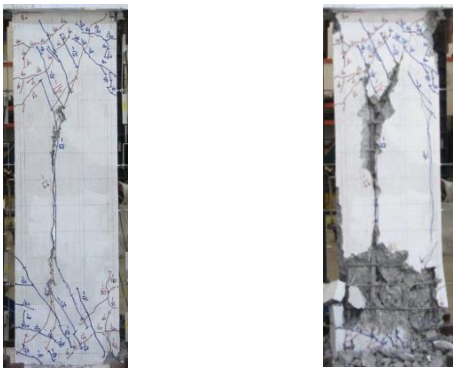

(a) at PL3 (b) at PL5

Fig. 10 Cracking patterns of RC-1.7-0.50

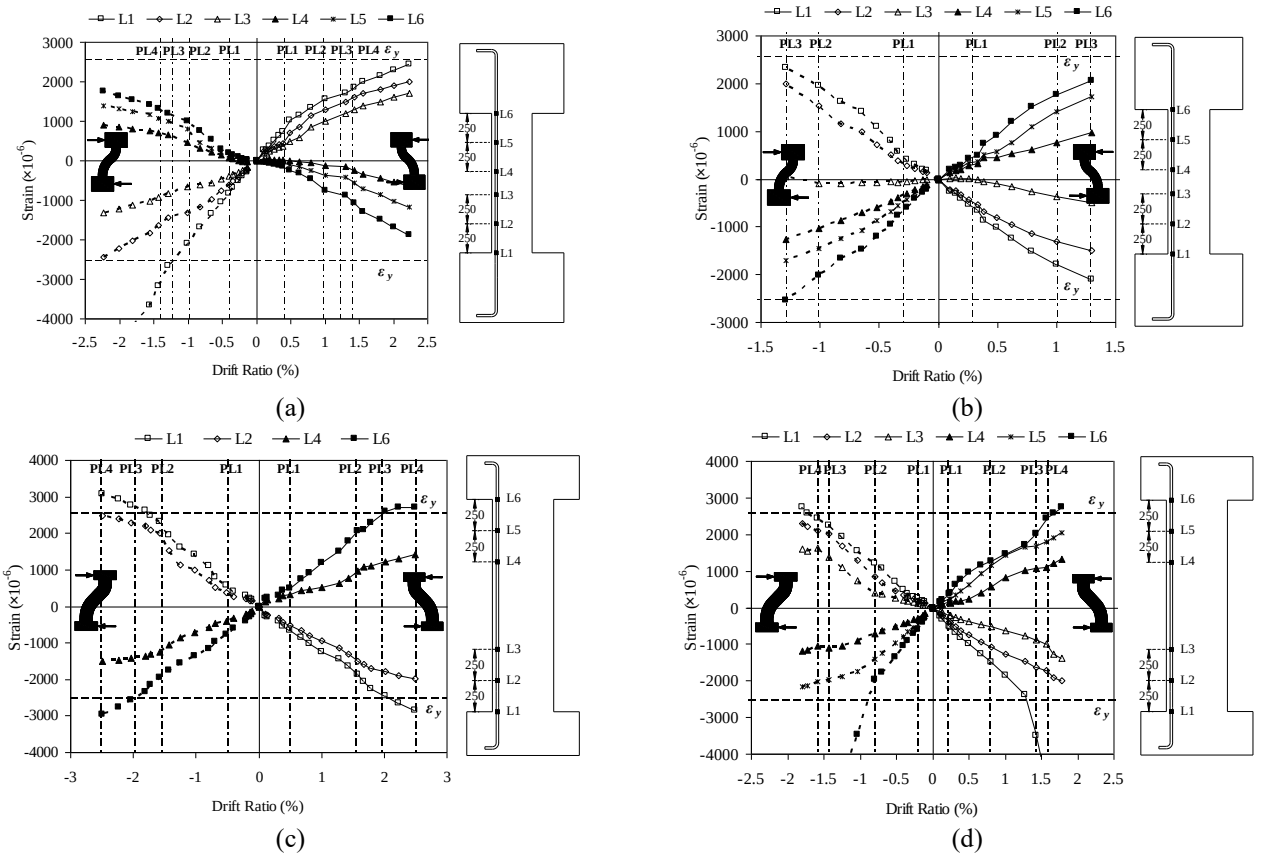

Fig. 11 Local strains in longitudinal reinforcing bars of test specimens

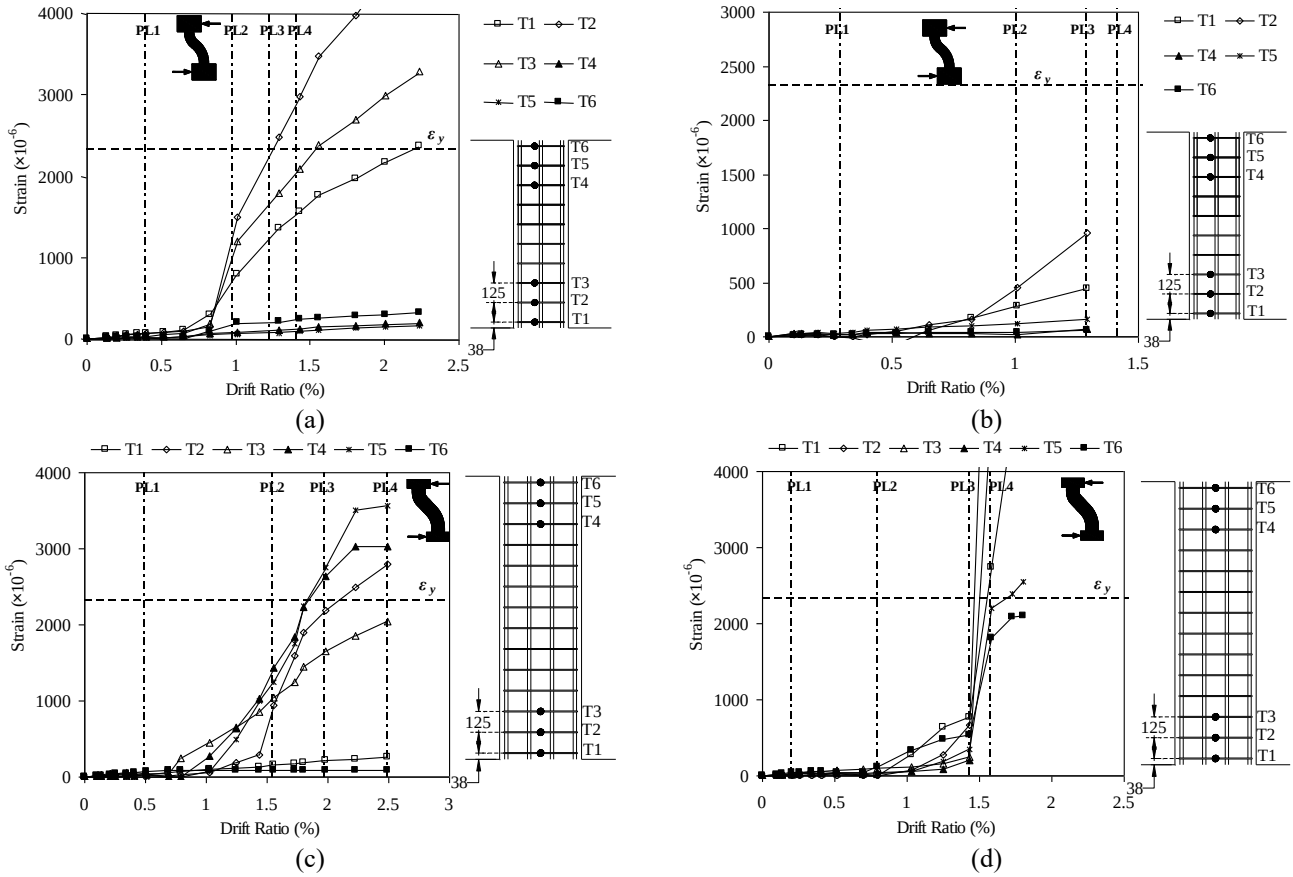

Fig. 12 Local strains in transverse reinforcing bars of test specimens

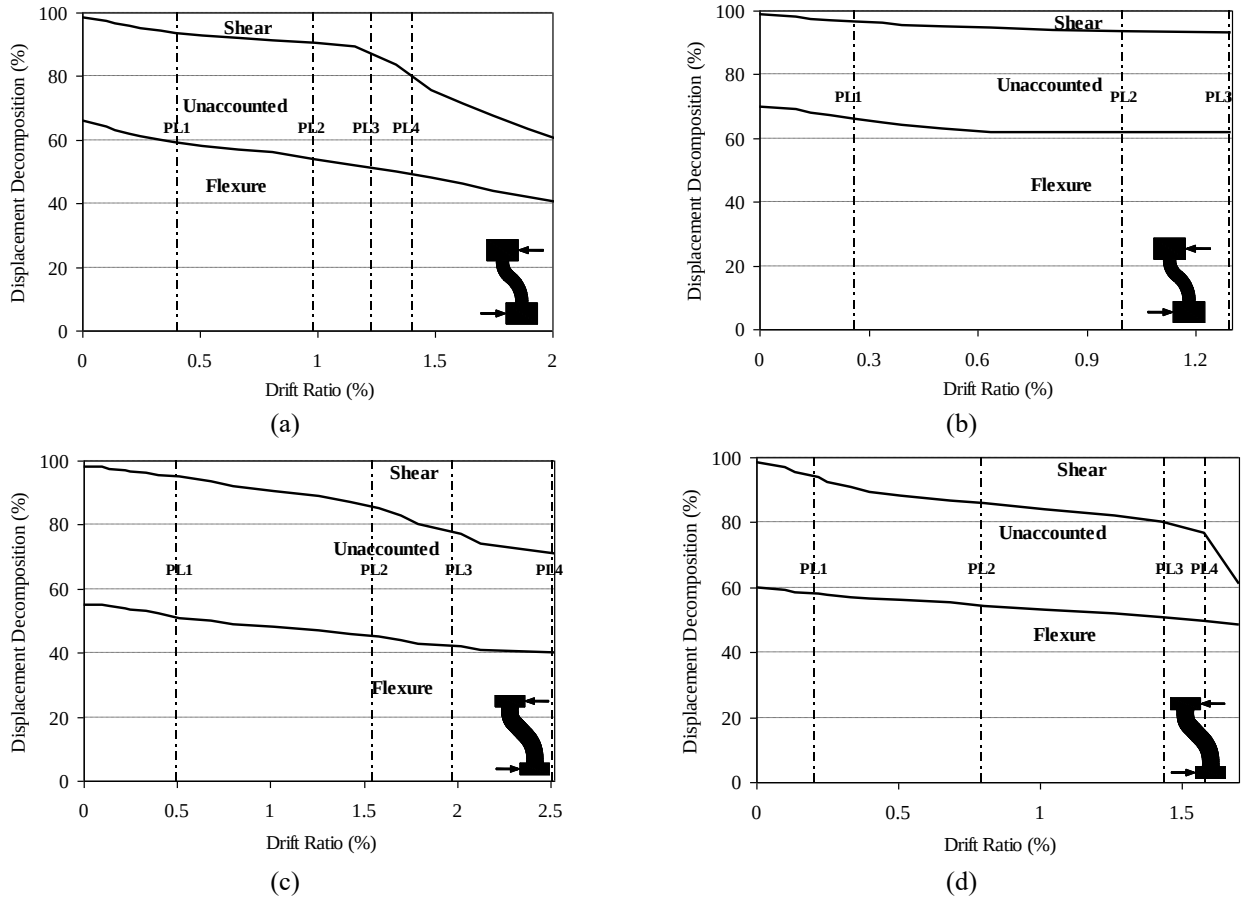

Fig. 13 Displacement decompositions of test specimens

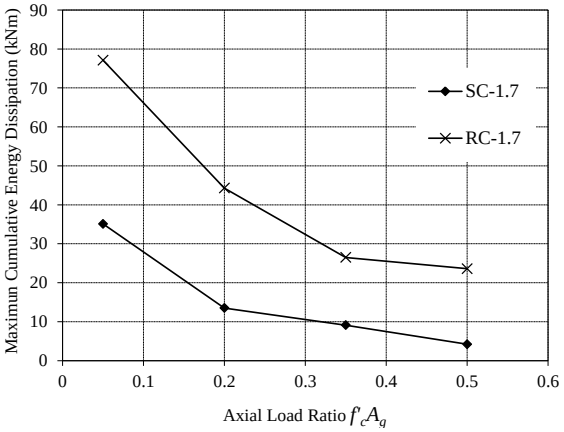

Fig. 14 Comparison of energy dissipation capacity among test specimens

presented together with performance levels as shown in Fig. 5. Five performance levels (PL) at five significant parts of the test were identified. They are the drift ratio (DR) at which the cracking shear force (V_{cr}) is attained (PL1); drift ratio at which the theoretical yield force (V_y) is reached (PL2); drift ratio at which the maximum shear force (V_{max}) is attained (PL3); drift ratio at which the shear-resisting capacity drops more than 20% of V_{max} (PL4) and drift ratio at which the test specimen is unable to sustain the constant applied column axial load (PL5).

Fig. 6 shows the measured horizontal story shear force versus horizontal displacement hysteresis loops of all specimens. The crack patterns in each test observed during the test were shown in Figs. 7 to 10. Figs. 11 and 12 exhibit the tensile strain profiles at the peak displacements of each drift ratio for the column longitudinal and transverse bars, respectively. Figs. 13 and 14 illustrate the energy dissipation capacity and the displacement decomposition of the specimens, respectively.

3.1 Specimen SC-1.7-0.05

In SC-1.7 Series with an aspect ratio of 1.7, Specimen SC-1.7-0.05 had the smallest applied column axial load of $0.05f'_cA_g$. Fig. 6(a) shows the hysteretic response together with the flexural strength and nominal shear strength of Specimen SC-1.7-0.05. A typical pinching behavior of shear-critical columns was observed throughout the test of Specimen SC-1.7-0.05. The specimen exceeded its yield force of 248.7 kN at a DR of 0.98% in the negative loading direction. The maximum shear force attained was approximately 276.4 kN, which was 91.2% of its theoretical flexural strength, corresponding to a DR of 1.23% in the positive direction. A sudden loss of shear-resisting capacity was observed at a DR of approximately 1.41% in both loading directions. At this stage, the attained shear forces were approximately 115.0 kN in the positive loading direction and 150.9 kN in the negative loading direction. In the subsequent loading cycles, the shear-resisting capacity

reduced gradually. During the first cycle of a DR of 11.29%, the specimen was unable to sustain its applied column axial load, which led to the test being stopped.

As shown in Fig. 7, in loading to a DR of 0.41%, hairline flexural cracks were developed at the bottom of the column. These flexural cracks propagated till a DR of 0.66%. In the subsequent loading cycles, fine shear cracks occurred at both ends of the column. No new flexural crack was found at this stage.

In loading to a DR of 1.41% (PL4), steeper diagonal shear cracks were formed in the middle of the specimen, which led to a sudden loss of shear-resisting capacity. Damages associated with these diagonal shear cracks included the fracture of transverse reinforcing bars, buckling of longitudinal reinforcing bars and crushing of concrete along these wide cracks. In loading to a DR of 11.29%, the specimen was unable to resist the applied column axial load, which led to the termination of the test.

The recorded strains along the longitudinal and transverse reinforcing bars of Specimen SC-1.7-0.05 are shown in Fig. 11(a) and 12(a), respectively. At a DR of 2.23%, a majority of strain gauges was damaged due to the crushing and spalling of concrete at the column interface together with severe diagonal cracking at both ends of the specimen. Therefore, the strain profiles of the reinforcing bars were only shown up to a DR of 2.23%. The recorded strains along the longitudinal reinforcing bars in Specimen SC-1.7-0.05 increased gradually as drift ratios increased. The largest tensile strain of 2450 μ was recorded at Location L1. It was slightly smaller than the yield strain of 2545 μ. The compressive yielding was observed at Location L1 during the loading to a DR of 1.29%. Yielding in the transverse reinforcing bars was first occurred at a DR of 1.29%. The largest tensile strain was detected at T2 Location. The strains in the transverse reinforcing bars increased significantly at a DR of 1.00% due to the occurrence of diagonal shear cracks along the specimen.

It is to be noted that at a DR of 2.0%, crushing and spalling of concrete at both ends of the column together with severe diagonal cracking along the column induced false readings on a majority of the measuring devices. Therefore, the displacement decompositions were only shown up to a DR of 2.0%. Fig. 13(a) shows the displacement decompositions of Specimen SC-1.7-0.05. Approximately 44 to 66% of total lateral displacement was contributed by the flexural deformation component, whereas 1.5 to 40.5% was accounted for by the shear deformation component. The cumulative energy absorbed by Specimen SC-1.7-0.05 is shown in Fig. 14. The total energy absorbed by Specimen SC-1.7-0.05 was 35.1 kNm. At a DR of 1.23%, at which the maximum shear force occurred in the positive loading direction, the absorbed energy was 4.24 kNm, which was only 12.1% of the total energy.

3.2 Specimen SC-1.7-0.50

Amongst all specimens in SC-1.7 Series, Specimen SC-1.7-0.50 had the highest applied column axial load of $0.50f'_cA_g$. The hysteretic response of Specimen SC-1.7-0.50 is plotted in Fig. 6(b). Specimen SC-1.7-0.50 showed a typical brittle shear failure and axial failure behaviors of reinforced concrete columns with light transverse reinforcement and a high column axial load. A maximum shear force of 375.6 kN was obtained by Specimen SC-1.7-0.50 at a DR of 1.25%. The higher maximum shear force by approximately 35.9% achieved in Specimen SC-1.7-0.50 as compared to Specimen SC-1.7-0.05 was due to the effects of the column axial load. The applied shear force in Specimen SC-1.7-0.50 exceeded its theoretical flexural strength at a DR of 1.25% in the negative loading direction. The lateral and axial loading resistance of the specimen was lost immediately after the specimen reached its maximum shear force. The ultimate recorded drift ratio obtained by the specimen was 1.42%. The test was then terminated at this stage.

Cracking patterns of Specimen SC-1.7-0.50 are shown in Fig. 8. At a DR of 0.26%, where the applied shear force exceeded the cracking force (PL1), there were no cracks formed. This could be due to the effects of a high axial load applied to the column of the specimen. In loading to a DR of 0.67% the first flexural cracks formed at the bottom of column. In the subsequent loading run, these cracks propagated inward and started inclining. At a DR of 1.01% (PL2), extensive diagonal shear cracks with an angle of more than 45^o formed at both top and bottom of the column. In loading to a DR of 1.25%, the cracking pattern of the specimen remained unchanged. In loading to a DR of 1.42% (PL4, PL5), a wide shear cracks suddenly occurred, extending from top to bottom of the column. The fracture of transverse reinforcing bars and buckling of longitudinal reinforcing bars along the shear crack were occurred simultaneously with the formation of this crack, which led to the shear failure and axial failure of the specimen and the termination of the test.

A majority of strain gauges was damaged due to the crushing and spalling of concrete at the column interface together with severe diagonal cracking at both ends of the specimen at a DR of 1.25%. Therefore, the recorded strains of reinforcing bars were only shown up to a DR of 1.25%. The strain profiles along the longitudinal reinforcing bar of Specimen SC-1.7-0.50 are shown in Fig. 11(b). In loading to a DR of 1.25% (PL3), the strain at L6 Locations was yielded compressively. Tensile yielding of the longitudinal reinforcing bars was not observed throughout the test. This was attributed to the effects of a high column axial force applied to the specimen. The measured strains in the transverse reinforcing bars of Specimen SC-1.7-0.50 are illustrated in Fig. 12(b). It is to be noted the strain gauge at T3 Location is inoperative, possibly damaged during the casting process, which resulted in the missing data. The largest strain was detected at Location T2. The recorded strains in the transverse reinforcing bars were relatively small up to a DR of 1.25% (PL3). The largest recorded strain up to this stage was only 961 μ. This complied with the cracking pattern at this stage (PL3), where little shear cracks were found.

Fig. 13(b) illustrates the contribution of displacement components at the peak displacements of Specimen SC-1.7-0.50. The major source of total lateral displacements was the flexure deformation. It is to be noted that at a DR of 1.25%, crushing and spalling of concrete at both ends of the

column together with severe diagonal cracking along the column induced false readings on a majority of the measuring devices. Therefore, the displacement decompositions were only shown up to a DR of 1.25%. Fig. 14 shows the cumulative absorbed energy of Specimen SC-1.7-0.50. The total energy absorbed up to the point of axial failure was 4.16 kNm.

3.3 Specimen RC-1.7-0.05

The major difference between RC-1.7 Series and SC-1.7 Series was the cross sectional dimension as the previous part. RC-1.7 Series consisted of specimens with a cross sectional dimension of 250 mm×490 mm, whereas the specimens in SC-1.7 Series had a cross sectional dimension of 350 mm×350 mm. In RC-1.7 Series, Specimen RC-1.7-0.05 had the smallest column axial load of $0.05f'_cA_g$. As shown in Fig. 6(c), the shear force increased steadily with an increase in the applied lateral displacement. Up to a DR of 0.50%, no changes in the gradient of slope were observed. The specimen reached its theoretical yield force at a DR of 1.55% in both loading directions. A maximum shear force of 283.1 kN was obtained in the specimen at a DR of 1.98% in the positive loading direction. This was equivalent to 101.4% of its theoretical flexural strength. In loading to a DR of 2.22%, a decrease in shear force was recorded. This decrease in shear force exceeded 20% of the maximum shear force at a DR of 2.49%. In the subsequent loading cycles, the specimen showed a gradual decrease in shear force with an increase in the applied lateral displacement. In loading to a DR of 11.3%, the shear-resisting capacity of the specimen was only 20.5 kN, equivalent to 7.2% of its maximum shear force. Axial failure also occurred at this drift ratio. The test was then terminated at this stage.

Fig. 9 shows the cracking patterns at each of the performance levels together with the corresponding drift ratios of the specimen. When loading to a DR of 0.50% (PL1), fine flexural cracks were initiated at both ends of the column. Flexural cracks propagated horizontally in the columns with a slight sign of shear inclination observed at the top of the column. No shear cracks were observed at this stage.

In loading to a DR of 1.55% (PL2), shear cracks propagating from the flexural cracks at both ends of the column were first observed. This was followed by more diagonal shear cracks at approximately 45°. In loading to a DR of 1.98% (PL3), extensive shear cracks with an inclined angle of more than 45° were observed at both ends of the column. No new flexural cracks were formed at this stage. Bond splitting cracks were developed at the middle of the column along the centered longitudinal reinforcing bar. In loading to a DR of 2.49% (PL4), the bond splitting cracks along the centered longitudinal reinforcing bar were appeared visibly. A new bond splitting cracks was formed along the side longitudinal reinforcing bar. No new shear and flexural cracks were observed at this stage. In loading to a DR of 11.3%, spalling of concrete cover along the bond splitting crack was observed. Crushing of concrete together with fracturing of transverse reinforcing bars along the diagonal shear cracks was recorded. At this stage, the specimen had reached its axial failure.

The measured strains in the longitudinal reinforcing bar of Specimen RC-1.7-0.05 are illustrated in Fig. 11(c). It is to be noted the strain gauges at L3 and L5 Locations are inoperative, possibly damaged during the casting process, which resulted in the missing data. A majority of strain gauges was damaged due to the crushing and spalling of concrete at the column interface together with severe diagonal cracking at both ends of the specimen at a DR of 2.49%. Therefore, the recorded strains of reinforcing bars were only shown up to a DR of 2.49%. It can be seen that as drift ratios increased, strains in the longitudinal reinforcing bars increased gradually. Tensile and compressive yielding was observed at L1 and L6 Locations when the drift ratio exceeded 1.98% (PL3). In loading to a DR of 2.49% (PL4), the tensile strain in the longitudinal reinforcing bar at L2 Location almost reached the yield strain of 2545 μ.

The measured strains in the transverse reinforcing bars of Specimen RC-1.7-0.05 are illustrated in Fig. 12(c). The locations of the strain gauges are also plotted in Fig. 4. The strains at T1 and T6 Locations were very small throughout the test. It complied with the cracking patterns as shown in Fig. 9, where little shear cracks were found at these locations. The strains in transverse reinforcing bars were relatively small up to a DR of 1.03%. The largest strain in transverse reinforcing bars at this stage was 634 μ. In the subsequent drift ratio, a drastic increase in strains was observed. It is to be noted that at this stage extensive shear cracks occurred at both ends of the column. The sudden increase in strains was due to the occurrence of these shear cracks. In loading to a DR of 1.98% (PL3), yielding was observed at T4 and T5 Locations. The strain at T2 Location was almost reached the yield strain at this stage. At a DR of 2.49% (PL4), the strain at T2 Location exceeded the yield strain.

Fig. 13(c) shows the contribution of deformation components expressed as percentages of the total lateral displacements at the peak displacements during each displacement cycle of Specimen RC-1.7-0.05. It is to be noted that crashing and spalling of concrete at both ends of the column together with severe diagonal cracking along the column induced false readings on a majority of the measuring devices at a DR of 2.49%. Therefore, the displacement decompositions were only shown up to a DR of 2.49%. The results indicated that approximately 40 to 55% of the total lateral displacement was due to flexure. The shear displacement component was relatively small up till a DR of 1.0%. In loading to a DR of 1.98% (PL3), the shear displacement component increased significantly. At a DR of 2.49%, at which shear strength degradation became severe (PL4), the shear displacement component reached approximately 29% of the total lateral displacement. The cumulative energy absorbed by Specimen RC-1.7-0.05 is shown in Fig. 14. The total energy absorbed of Specimen RC-1.7-0.05 was 77.1 kNm, which was higher than that of Specimen SC-1.7-0.05. At a DR of 1.98%, at which the maximum shear force occurred in the positive loading direction, the cumulative absorbed energy was 21.7 kNm, equivalent to 28.1% of the total energy absorbed; and at a DR of 1.98% (PL4), it was 40.8% of the total energy absorbed.

3.4 Specimen RC-1.7-0.50

Amongst all specimens in RC-1.7 Series, Specimen RC-1.7-0.50 had the highest applied column axial load of $0.50f'_cA_g$. The shear force versus lateral displacement response of Specimen RC-1.7-0.50 is plotted in Fig. 6(d). A gradual increase in the shear force of the specimen with an increase in the applied lateral displacement was observed up to PL2 (a DR of 0.79%). After that, a decrease in the gradient of the backbone curve was observed. A maximum shear force of 355.2 kN was recorded at a DR of 1.44% (PL3) in the negative loading direction. Specimen RC-1.7-0.50 depicted a brittle shear failure behavior. The shear-resisting capacity of Specimen RC-1.7-0.50 was suddenly reduced at a DR of 1.67% just after the maximum shear force was reached. This was followed by a gradual decrease in the shear strength of the test specimen. At a DR of 1.80%, the specimen reached its axial failure.

The cracking patterns at two critical performance levels together with the corresponding drift ratios of Specimen RC-1.7-0.50 are shown in Fig. 10. Generally, similar trends of the cracking patterns were observed in Specimen RC-1.7-0.50 as compared to that observed in Specimen RC-1.7.0.05. Hairline flexural cracks were developed at both ends of the column at a DR of 0.20% (PL1). Flexural cracks propagated horizontally in the columns with no sign of shear inclination observed at both ends of the column till a DR of 0.79% (PL2). In loading to a DR of 1.44% (PL3), severe shear cracking was initiated at both ends of the column. In loading to a DR of 1.67% (PL4), the bond splitting crack along the centered longitudinal reinforcing bar were observed in the middle of the column along the centered longitudinal reinforcing bar. This crack was the extension of the existing shear crack at the top of the column. New diagonal cracks with a steep angle were also found at stage. In loading to a DR of 1.80% (PL5), significant spalling of concrete cover along both sides of the bottom of column together with crushing of concrete at the bottom was observed. Fracturing of transverse reinforcing bars together with buckling of longitudinal reinforcing bars at the bottom of column was also seen at this stage.

The measured strains in the longitudinal reinforcing bars of Specimen RC-1.7-0.50 are illustrated in Fig. 11(d). With reference to this strain profile, tensile yielding of the longitudinal reinforcing bars was observed up till a DR of 1.67%; whereas compressive yielding was occurred at a DR of 1.03%. Fig. 12(d) shows the recorded strains in the transverse reinforcing bars of Specimen RC-1.7-0.50. Yielding was first occurred at a DR of 1.57%. The strains in the transverse reinforcing bars increased significantly at a DR of 1.57% due to the occurrence of diagonal shear cracks along the specimen.

Fig. 13(d) shows the displacement decompositions of Specimen RC-1.7-0.50. Approximately 48 to 60% of the total lateral displacement was contributed by the flexural deformation component, whereas 2 to 39% was accounted for by the shear deformation component. The cumulative energy absorbed by Specimen RC-1.7-0.50 is shown in Fig. 14. The total energy absorbed up to the axial failure stage was 23.6 kNm.

Table 2 Comparison with the existing initial models

Specimen	$K_{i\text{-}exp}$ kN/mm	$\frac{K_{i-\exp}}{K_{i-EE}}$	$\frac{K_{i-\exp}}{K_{i-Tran}}$	$\frac{K_{i-\exp}}{K_{i-ELwood}}$
SC-1.7-0.05	24.5	0.560	0.918	0.372
SC-1.7-0.20	26.9	0.590	0.865	0.295
SC-1.7-0.35	28.8	0.553	0.653	0.239
SC-1.7-0.50	34.4	0.507	0.620	0.220
RC-1.7-0.05	11.5	0.365	0.898	0.242
RC-1.7-0.20	15.4	0.442	0.846	0.244
RC-1.7-0.35	18.9	0.391	0.661	0.221
RC-1.7-0.50	21.4	0.348	0.583	0.197
Mean		0.47	0.756	0.254
Coefficient of Variation		0.095	0.139	0.056

4. Discussion and comparison

The test results of four RC short columns with light transverse reinforcement were reported individually in the previous part. In this part of the paper, further discussion and investigation will be carried out to establish deeper understanding of the seismic behavior of the short RC columns with light transverse reinforcement subjected to seismic loadings. Selected results from all test specimens in this experimental program and Tran and Li (2015)'s ones will be compared in this part to determine the effects of column axial load to the seismic behavior of RC short columns with light transverse reinforcement. The obtained results of all test specimens are also compared with existing initial stiffness, shear strength and drift ratio at axial failure models.

4.1 Initial stiffness

The backbone curves were used to calculate the initial stiffness of the test specimens. The initial stiffness is calculated corresponding to the theoretical yield force, which is defined as either the longitudinal reinforcement reaches its yield strain or when the compressive strain in the concrete reaches a value of 0.002. This definition could only be applicable for specimens with shear strengths substantially exceeding its theoretical yield force. For other cases, defined as those whose maximum measured shear force was less than 107% of the theoretical yield force, the initial stiffness was defined based on a point on its backbone curves with a shear force that equates to 80% of the obtained maximum shear force.

The relationships between initial stiffness and the column axial load ratio of all test specimens are plotted in Fig. 15. The initial stiffness of SC-1.7 Series specimens were enhanced by around 9.8%, 17.6%, and 40.4% as the column axial load was increased from 0.05 to 0.20, 0.35, and $0.50f'_cA_g$, respectively. An analogous trend was observed in the specimens of RC-1.7 Series, whose initial stiffness experienced an enhancement of around 33.9%, 64.3% and 86.1% with an increase in the column axial load from 0.05 to 0.20, 0.35 and 0.50 f'_cA_g, respectively.

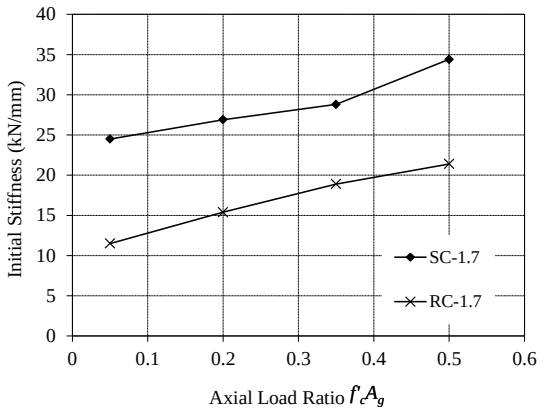

Fig. 15 Comparison of initial stiffness between test specimens

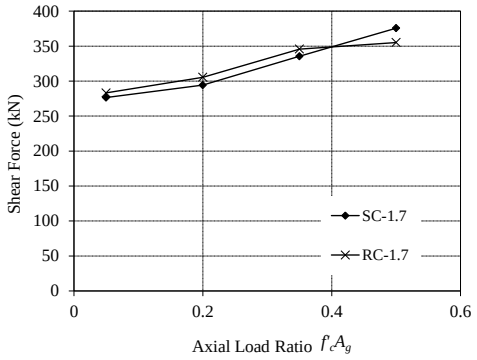

Fig. 16 Comparison of shear strength between test specimens

Elwood and Eberhard (2009) define the initial stiffness of reinforced concrete columns as follows

$$k = \frac{0.45 + 2.5P / A_g f_c^{'}}{1 + 110\left(\frac{d_b}{h}\right)\left(\frac{h}{a_s}\right)} \le 1 \quad \text{and} \quad \ge 0.2 \tag{1}$$

where h is the column depth; a_s is the shear span and d_b is the diameter of longitudinal reinforcing bars.

Tran and Li (2012) used strut-and-tie method to derive a model for the initial stiffness of RC columns. The stiffness ratio of RC columns in Tran and Li (2012)'s model is calculated as

$$\kappa = \left(2.043R_n^2 + 2.961R_n + 1.739\right)\left(3.023R_a + 2.573\right) \tag{2}$$

where the aspect ratio (R_a) and axial load ratio (R_n) are equal to a_s/d and P/f'_cA_g, respectively.

The stiffness ratio is

$$\kappa = \frac{I_e}{I_g} \times 100\% \tag{3}$$

The measured effective moment of inertia is defined as

$$I_e = \frac{L^3 K_i}{12E_c} \tag{4}$$

where E_c is the elastic modulus of concrete; I_g is the moment of inertia of the gross section; L is the height of columns and K_i is the initial stiffness of columns.

As shown in Table 2, it was found that the initial stiffness models developed by Elwood and Eberhard (2009) and Tran and Li (2012) produced better results than the existing seismic assessment guidelines (Elwood *et al.* 2007). Comparing between Elwood and Eberhard's (2009), and Tran and Li's model (2012), Tran and Li's model (2012) produced a better mean ratio of the experimental to predicted initial stiffness than Elwood and Eberhard's one (2009).

4.2 Shear strength

Fig. 16 plots the shear strength versus the column axial load ratio of all test specimens. The column axial load in the test specimen varied from 0.05 to $0.50f'_cA_g$. As observed in Fig. 16, as the ratio of column axial load was changed from 0.05 to 0.20, 0.35, and 0.50; the shear strength of SC-1.7 Series specimens increased by around 6.4%, 21.4%, and 35.9%, respectively. The tested results of specimens of RC-1.7 Series showed a similar trend. The shear strengths of RC-1.7 Series specimens exhibited an increase of around 7.9% and 22.1% with an increase in the ratio of column axial load from 0.05 to 0.20 and $0.35f'_cA_g$, respectively. However, a slight increase of 2.7% in the shear strength was observed in RC-1.7 Series specimens, as the column axial load was increased from 0.35 to $0.50f'_cA_g$. It is to be noted that Specimen RC-1.7-0.50 had the smallest ratio of theoretical flexural strength to nominal shear strength.

Between the specimens of SC-1.7 and RC-1.7 Series, an increase in the shear strength of 2.4%, 3.8%, and 3.0% was recorded for the specimens with an axial load of 0.05, 0.20, and $0.35f'_cA_g$ respectively. This could be attributed to the longer depth of RC-1.7 Series specimens as compared to SC-1.7 Series specimens. For the same shear crack angle, the longer the depth of the column is, the more the number of the transverse reinforcing bars crosses the shear crack, which leads to the higher transverse reinforcement contribution to the shear strength. In addition, both RC-1.7 Series and SC-1.7 Series specimens had the same cross sectional area and aspect ratio. Therefore, the same concrete contribution to the shear strength was expected in both RC-1.7 Series and SC-1.7 Series specimens. As compared with Specimen SC-1.7-0.50, Specimen RC-1.7-0.50 obtained the lower shear strength. As explained previously, the maximum shear force of Specimen RC-1.7-0.50 was controlled by the flexural strength, which then led to this result.

According to both ACI 352 (2002) and ASCE/SEI 41's suggestion (2007), the maximum shear force of the column is limited by its shear strength. Where the shear strength as defined in both ACI 352 (2002) and ASCE/SEI 41's suggestion (2007) is given as

$$V_n = k_1 \frac{A_v f_{yt} d}{s} + \lambda k_2 \left(\frac{0.5\sqrt{f_c^{'}}}{a/d} \sqrt{1 + \frac{P}{0.5\sqrt{f_c^{'}} A_g}} \right) 0.8A_g \tag{5}$$

(MPa)

where $k_1$is equal to 1 for transverse steel spacing less than or equal to d/2, k_1 is equal to 0.5 for spacing exceeding d/2 but not more that d, k_1 is equal to 0 otherwise; k_2 is taken as 1 for displacement ductility less than 2, as 0.7 for displacement ductility more than 4 and varies linearly for intermediate displacement ductility; a/d shall not be taken greater than 3 or less than 2; and λ is equal to 1 for normal-weight concrete.

As shown in Table 1, both ACI 352 (2002) and ASCE/SEI 41's suggestion (2007) provided a good prediction of the shear strength of the test specimens.

4.3 Drift ratio at axial failure

Fig. 17 shows the drift ratio at axial failure versus the column axial load ratio of the test specimens. The general trend of the curves in Fig. 17 showed that an increase in the column axial load ratio reduced the drift ratio at axial failure in all test series.

As observed in Fig. 17, the drift ratio at axial failure in SC-1.7 and RC-1.7 Series specimens reduced sharply by around 83.9% and 74.6% respectively as the column axial load ratio was increased from 0.05 to 0.20. However, only a slight decrease of 14.3% and 29.6% in the drift ratio at axial failure was recorded in SC-17 and RC-1.7 Series specimens respectively, as the column axial load was increased from 0.20 to $0.35f'_cA_g$. Further increasing the column axial load from 0.35 to $0.50f'_cA_g$, similar trend was obtained in both SC-1.7 and RC-1.7 Series. Based on the aforementioned discussion, it is concluded that the column axial load had detrimental effects on the drift ratio at axial failure.

For an axial load ratio of 0.05, a slightly higher drift ratio at axial failure was observed in the SC-1.7 as compared to RC-1.7 specimen. The higher drift ratio at axial failure of 57.6%, 29.5% and 26.8% was recorded in the specimen of RC-1.7 Series as compared to SC-1.7 Series for an axial load ratio of 0.20, 0.35 and 0.50 respectively. This observed trend was suggested to be due to the difference in the mode of axial failure of the test specimens. It is to be noted that both Specimen RC-1.7-0.05 and SC-1.7-0.05 shared the same mode of axial failure, where the axial failure in the specimens was attributed to the extended damaged zone. While for an axial load ratio of 0.20 and 0.50, different modes of axial failure were observed in the specimens of RC-1.7 and SC-1.7 Series.

Based on the shear friction model, Elwood and Moehle (2005) derived the following equation for the drift ratio at axial failure

$$\left(\frac{\Delta}{L}\right)_a = \frac{4}{100}\frac{1+(\tan\theta)^2}{\tan\theta + P\left(\dfrac{s}{A_{st}f_{yt}d_c\tan\theta}\right)} \tag{6}$$

where f_{yt} is yield strength of transverse reinforcement; A_{st} is total transverse reinforcement area within spacing s; θ is angle of diagonal crack; d_c is the depth of core.

Based on the energy analogy and the experimental database, a model for the ultimate displacement of RC columns with light transverse reinforcement had been developed by Tran and Li (2013). This ultimate displacement is defined as follows

Table 3 Comparison with the existing ultimate displacement models

Specimen	$(\Delta_a)_{exp}$	$(\Delta_a)_{Elwood}$	$(\Delta_a)_{Tran}$	$\frac{(\Delta_a)_{exp}}{(\Delta_a)_{Elwood}}$	$\frac{(\Delta_a)_{exp}}{(\Delta_a)_{Tran}}$
SC-1.7-0.05	135.5	69.9	205.1	1.938	0.601
SC-1.7-0.20	21.8	31.5	28.8	0.692	0.757
SC-1.7-0.35	18.7	21.5	14.4	0.87	1.299
SC-1.7-0.50	17.0	14.8	14.0	1.149	1.214
RC-1.7-0.05	192.5	116.1	315.2	1.658	0.611
RC-1.7-0.20	48.8	45.3	47.5	1.078	1.027
RC-1.7-0.35	34.4	23.8	23.8	1.215	1.445
RC-1.7-0.50	30.6	21.5	16.9	1.426	1.811
Mean				1.253	1.096
Coefficient of Variation				0.408	0.429

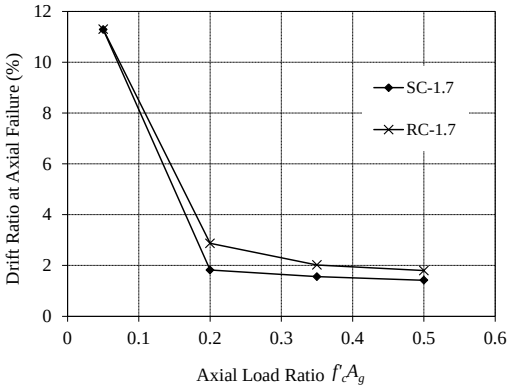

Fig. 17 Comparison of drift ratio at axial failure between test specimens

$$\left(\frac{\Delta}{L}\right)_a = \frac{4}{100}\frac{1+(\tan\theta)^2}{\tan\theta + P\left(\dfrac{s}{A_{st}f_{yt}d_c\tan\theta}\right)} \tag{7}$$

$$\Delta_a = 2\Delta_y + \delta_a^* h\tan\theta$$

$$P = \rho_l bh\left(\frac{f_{yl}}{0.2874\times\delta_a^*+1}\right)\frac{1}{\sin\theta} + \frac{df_{yt}A_{st}}{s} + k\sqrt{f'_c}(0.8A_g)\cot\theta \tag{8}$$

where f_{yl} is yield strength of longitudinal bars; A_g is cross sectional area; ρ_l is ratio of longitudinal reinforcement; Δ_y is yield displacement; k is displacement ductility demand parameter.

As shown in Table 3, the mean ratios of the experimental to the predicted displacement at axial failure and its coefficient of variation are 1.253 and 0.408 for Elwood and Moehle's model (2005), 1.096 and 0.429 for Tran and Li's model (2013), respectively. Comparing the existing models with experimental data indicates that Tran and Li's model (2013) produced a better mean ratio of the experimental to predicted displacement at axial failure than Elwood and Moehle's model (2005), however the coefficient of variation of Tran and Li's model (2013) is higher than Elwood and Moehle's model (2005). Tran and Li's model (2013) has the tendency to underestimate and

overestimate the displacement at axial failure for specimens with a high column axial load and low column axial load, respectively.

5. Conclusions

An experimental program carried out on four reinforced concrete short columns with light transverse reinforcement to the point of axial failure was presented. The variables in the test specimens include column axial loads and cross sectional shapes. The test results are compared with experimental data conducted by Tran and Li (2015). The conclusions drawn from the current experimental investigations are as follows:

• The drift ratio at axial failure and maximum energy dissipation capacity of the tested specimens were increased as the column axial load increased.

• The column axial load had a beneficial effect on the shear strength and initial stiffness of the tested specimens.

• The shear strength following ASCE/SEI 41 (2007) provided a good estimation of the results obtained from the tested specimens.

• Tran and Li's model (2012) based on strut-and tie method provided a good prediction of the initial stiffness of the test specimens.

• Tran and Li's model (2013) has the tendency to underestimate and overestimate the displacement at axial failure for specimens with a high column axial load and low column axial load, respectively.

Acknowledgments

This research is funded by Vietnam National Foundation for Science and Technology Development (NAFOSTED) under grant number 107.01-2016.04.

References

ACI 352 (2002), *Recommendations for Design of Beam-Column Joints in Monolithic Reinforced Concrete Structures*, Joint ACI-ASCE Committee 352, Farmington Hills, Michigan, U.S.A.

ASCE/SEI 41 (2007), *Seismic Rehabilitation of Existing Buildings*, American Society of Civil Engineers, Reston, Virginia, U.S.A.

EERI (2012), *The M_w 6.9 Sikkim-Nepal Border Earthquake of September 18, 2011*, EERI Special Earthquake Report, Oakland, California, U.S.A.

EERI (2013), *The November 7, 2012 M7.4 Guatemala Earthquake and Its Implications for Disaster Reduction and Mitigation*, A Joint Report of EERI and AGIES, Oakland, California, U.S.A.

EERI (2016), *M7.8 Gorkha, Nepal Earthquake on April 25, 2015 and Its Aftershocks*, EERI Earthquake Reconnaissance Team Report, Oakland, California, U.S.A.

EERI (2017), *M6.5 Pidie Jaya Earthquake Aceh Indonesia on December 7, 2016*, EERI Earthquake Reconnaissance Team Report, Oakland, California, U.S.A.

Elwood, K. and Moehle, J. (2005), "Axial capacity model for shear-damaged columns", *ACI Struct. J.*, **102**(4), 578-587.

Elwood, K., Matamoros, A.B., Wallace, J.W., Lehman, D.E., Heintz, J.A., Mitchell, A.D., Moore, M.A., Valley, M.T., Lowes, L.N., Comartin, C.D. and Moehle, J.P. (2007), "Update to ASCE/SE 41 concrete provisions", *Earthq. Spectr.*, **23**(3), 493-523.

Elwood, K. and Eberhard, M.O. (2009), "Effective stiffness of reinforced concrete columns", *ACI Struct. J.*, **106**(4), 476-484.

Ghannoum, W.M. and Moehle, J. (2012a), "Shake-table tests of a concrete frame sustaining column axial failures", *ACI Struct. J.*, **109**(3), 393-402.

Ghannoum, W.M. and Moehle, J. (2012b), "Dynamic collapse analysis of a concrete frame sustaining column axial failures", *ACI Struct. J.*, **109**(3), 403-412.

Koçak, A. (2013), "The effect of short columns on the performance of existing buildings", *J. Struct. Eng. Mech.*, **46**(4), 505-518.

Koçak, A. (2015), "Earthquake performance of FRP retrofitting of short columns around band-type windows", *J. Struct. Eng. Mech.*, **53**(1), 1-16.

LeBorgne, M.R. and Ghannoum, W.M. (2014), "Analytical element for simulating lateral-strength degradation in reinforced concrete columns and other frame members", *ASCE J. Struct. Eng.*, **140**(7), 04014038.

Lynn, A.C. (2001), "Seismic evaluation of existing reinforced concrete building columns", Ph.D. Dissertation, University of California, Berkeley, U.S.A.

Nakamura, T. and Yoshimura, M. (2002), "Gravity load collapse of reinforced concrete columns with brittle failure modes", *J. Asian Architect. Build. Eng.*, **1**(1), 21-27.

Ousalem, H. (2006), "Experimental and analytical study on axial load collapse assessment and retrofit of reinforced concrete columns", Ph.D. Dissertation, University of Tokyo, Tokyo, Japan.

Sezen, H. (2008), "Shear deformation model for reinforced concrete columns", *Struct. Eng. Mech.*, **28**(1), 39-52.

Sharma, A., Reddy, G.R. and Vaze, K.K. (2012), "Shake table tests on a non-seismically detailed RC frame structure", *Struct. Eng. Mech.*, **41**(1), 1-24.

Tran, C.T.N. (2012), "Modeling of non-seismically detailed columns subjected to reversed cyclic loadings", *Struct. Eng. Mech.*, **44**(2), 163-178.

Tran, C.T.N. and Li, B. (2012), "Initial stiffness of reinforced concrete columns with moderate aspect ratios", *Adv. Struct. Eng.*, **15**(2), 265-276.

Tran, C.T.N. and Li, B. (2013), "Ultimate displacement of reinforced concrete columns with light transverse reinforcement", *J. Earthq. Eng.*, **17**(2), 282-300.

Tran, C.T.N. and Li, B. (2015), "Experimental studies on the backbone curves of reinforced concrete columns with light transverse reinforcement", *J. Perform. Constr. Facilit.*, **29**(5), 04014126.

Wibowo, A., Wilson, J.L., Lam, N.T.K. and Gad, E.F. (2014), "Drift performance of lightly reinforced concrete columns", *Eng. Struct.*, **59**, 522-535.

Yoshimura, M. and Yamanaka, N. (2000), "Ultimate limit state of RC columns", *Proceedings of the 2nd US-Japan Workshop on Performance-Based Earthquake Engineering Methodology for Reinforced Concrete Building Structures*, Sapporo, Japan.

Yoshimura, M. and Nakamura, T. (2003), "Axial collapse of reinforced concrete short columns", *Proceedings of the 4th US-Japan Workshop on Performance-Based Earthquake Engineering Methodology for Reinforced Concrete Building Structures*, Toba, Japan.

Yoshimura, M., Takaine, Y. and Nakamura, T. (2003), "Collapse drift of reinforced concrete columns", *Proceedings of the 5th*

US-Japan Workshop on Performance-Based Earthquake Engineering Methodology for Reinforced Concrete Building Structures, Hakone, Japan.

CC